EMG-based Simultaneous Estimations of Joint Angle and Torque during Hand Interactions with Environments

Dongwon Kim[1], Kyung Koh[2], Giovanni Oppizzi[2,4], Raziyeh Baghi[2], Li-Chuan Lo[1], Chunyang Zhang[1], and Li-Qun Zhang[2-4]

[1]EpicWide, Baltimore, MD, USA,
[2]Department of Physical Department of Physical Therapy and Rehabilitation Science, University of Maryland, Baltimore, MD, USA,
[3]Department of Orthopaedics, University of Maryland, Baltimore, MD, USA
[4]Department of Bioengineering, School of Engineering, University of Maryland, College Park, MD, USA

***Abstract*—It is necessary to control contact force through modulation of joint stiffness in addition to the position of our limb when manipulating an object. This is achieved by contracting the agonist muscles in an appropriate magnitude, as well as, balancing it with contraction of the antagonist muscles. Here we develop a decoding technique that estimates both the position and torque of a joint of the limb in interaction with an environment based on activities of the agonist-antagonistic muscle pairs using electromyography in real time. The long short-term memory (LSTM) network that is capable of learning time series of a long-time span with varying time lags is employed as the core processor of the proposed technique. We tested both the unidirectional LSTM network and bidirectional LSTM network. A validation was conducted on the wrist joint moving along a given trajectory under resistance generated by a robot. The decoding approach provided an agreement of greater than 93% in kinetics (i.e. torque) estimation and an agreement of greater than 83% in kinematics (i.e. angle) estimation, between the actual and estimated variables, during interactions with an environment. We found no significant differences in performance between the unidirectional LSTM and bidirectional LSTM as the learning device of the proposed decoding method.**

***Index Terms*—Human-machine interaction, Electromyography (EMG), Decoding, Machine learning, Prosthesis.**

I. INTRODUCTION

IN usual interactions with an object, human behaviors are described in neither an isometric manner nor an isotonic manner. When grasping or manipulating an object, the human regulates the position of the limb, while maintaining appropriate contact force or stiffness to perform a given task. Torque to position the limb toward the target is produced by differences between contractions of agonist and antagonist muscles about a joint. Joint stiffness increases when both agonist and antagonist muscles are simultaneously activated. It may be necessary to consider both the position and stiffness (or contact force) in controlling robot manipulators or prosthetic devices that replace the user's limb.

Surface electromyography (EMG) is recognized as a preferred interface versus other input media including a joystick or a haptic device with which mechanism that the user should be acquaint [1-5]. Indeed, frequent attempts to use surface EMG to decode limb kinematics or kinetics have been made through pattern recognition or regression (mapping EMG to angle or force) for controlling prosthetic devices or teleoperated robots [6-11]. Despite the need of taking both kinematics and kinetics in design of interactive devices into account, only the isometric condition or isotonic condition is considered in most EMG-based control applications. Kinematic data or kinetic data were obtained with no resistance to motions of participants involved or with the joint angle entirely restricted. It may be thought to be less useful or less realistic for applications in interactive environments which typically drive force exertion as well as motion.

A few studies focused on simultaneous estimation schemes for joint angle and torque (stiffness) based on EMG signals. The majority of the simultaneous estimation schemes rely on mathematical models based on the intuitive fact [12-14]. These models predict the position of a joint based on the difference between flexor and extensor activations, while estimating stiffness using simultaneous activations of the flexor and extensor. Though these methods are capable of efficiently deciphering the user's intention, the prediction accuracy of these methods is relatively low [12-14]. A significant improvement was achieved in a study that adopted hidden variables to model unobserved and intrinsic system states between muscle activation and limb kinematics/kinetics, linking the hidden variables with muscle activation and limb kinematics/kinetics using an optimization technique [15].

Nowadays, machine learning is one of the exploding application fields that enables one to predict outcomes of interest in a robust and accurate way based on a trained

 Digital Object Identifier: 10.1109/TBME.2021.3134204

black box that maps the inputs to the outputs. Certainly, machine learning techniques have been a tool in developing EMG-based decoding methods. Several studies have demonstrated the excellent performance of machine learning techniques in myoelectrically driven applications using surface EMG [10, 16-21]. Still, these are restricted solely to decoding either kinematics or kinetics only, however. The purpose of this study is to develop a method for EMG-based decoding of both joint kinematics and kinetics utilizing the power of machine learning.

The time dependency of EMG signals is high; instantaneous EMG is also informative. It is a typical way to extract features from EMG signals with a time window of samples in a range between 50 ms and 500 ms [19, 22-24]. Storage of history of the related information is required for processing EMG accordingly. The recurrent neural network (RNN) is known as a suitable network for processing sequential data by transferring information across time steps via hidden states, which enables the history of a sequence to be stored in the networks. Traditional RNNs, however, expose a disadvantage of the requirement for time lags to be predetermined to learn temporal sequence processing [25]. RNNs may not be fully appropriate to capture human movements that are often aperiodic in daily life, though they are a reciprocating action. As a variant of RNN, the long short-term memory (LSTM) neural network was devised to learn time series with a long time span and determine optimal time lags for prediction [26]. Indeed, LSTM neural networks have produced successful applications in various areas with strong time dependency, including speech recognition [27] and human action recognition [28-30]. LSTM neural networks are an excellent candidate to decode human motion based on EMG signals. Recently, an EMG-based kinematics decoding method that combined LSTM neural network with convolutional neural network was proposed [19].

The proposed EMG decoding method of both joint kinematics and kinetics stands on unidirectional LSTM and bidirectional LSTM neural networks. We evaluate its performance in estimating the wrist angle and torque based on surface EMGs of a pair of wrist flexor and extensor muscles. While several magnitudes of resistance are imposed on the wrist joint by a robot, participants are asked to move their wrist joint according to given trajectories. To examine the efficacy of LSTM neural networks in learning time series with long time spans using varying time lags for prediction of the angle and torque of the wrist joint, we present different trajectories with irregularity and aperiodicity to the participants for the training and evaluation phases of the decoding procedure, respectively. This effort would provide an insight into the predictability of unlearned motions by the proposed technique based on learned motions. A comparison with a decoding method that possesses no device for time dependency of data demonstrates the proposed method's advantageous capability of learning a long time-span data for EMG-based decoding of kinematics and kinetics. Part of this study was presented in a conference [31].

II. Methods

A. Participants

The experiment was approved by the Institutional Review Board at the University of Maryland. All participants gave written informed consent. A total of 8 volunteers (4 female, 4 male), ranging in age from 23 to 41 years (33.25 ± 7.94 standard deviation), took part in the study. All participants reported that they had no neurological or motor deficit and that they were right-handed.

B. Apparatus

A one degree-of-freedom robot for the wrist joint was developed. The motor (LS Mecapion, APM-SA01ACN-8) embedded an encoder of a resolution of 2048 pulses per revolution and was connected with a Harmonic Drive gear with a ratio of 50:1. A torque sensor (Transducer Techniques, TRT-200) was installed between the Harmonic Drive and the hand plate. A custom Advanced Motion Controls (AMC) drive was used to convert the motor command into the current to the motor.

Two wireless pre-amplified surface EMG electrodes (Delsys, Trigno) were used to acquire EMG signals from the flexor carpi radialis (FCR), and extensor carpi radialis (ECR) muscles.

A monitor was placed in front of the participant with a distance of about half meter to display wrist flexion trajectories to follow. Fig. 1 displays the schematic of the experimental setup.

Data processing including feature extraction as well as data acquisition and motor control were conducted in a LabVIEW environment through a data acquisition card (Texas Instruments, PCI-6225). The sampling rate for all data was set at 1000 Hz.

The EMG-based decoder was developed and performed utilizing Matlab Deep Learning Toolbox™ (MathWorks, Matlab 2018b). EMG features calculated in the LabVIEW program were exchanged with estimated angle and torque

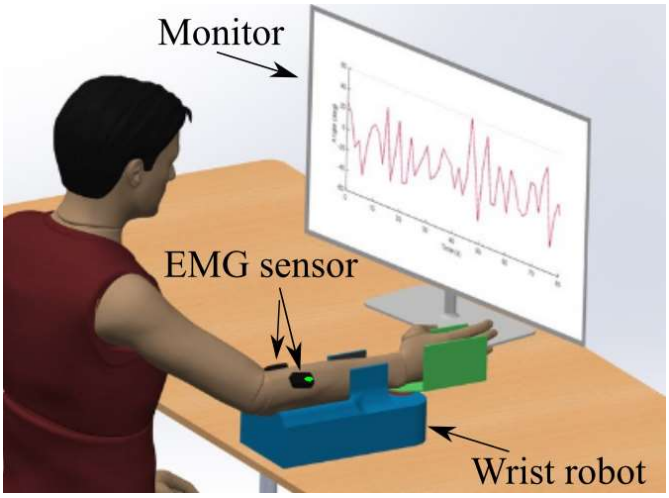

Fig. 1. Experimental setup: A participant sits on a chair with a specific arm configuration on the right side: 45 degree abduction and 45 degree flexion at the shoulder, 50 degree flexion at the elbow. Two wireless surface EMG electrodes are placed on the FCR and ECR muscles. A monitor displays the

produced in Matlab through UDP (User datagram protocol) communication.

C. Signal Processing

Raw EMG signals were differenced prior to feature extraction, since differencing enables EMG signals to be more stationary than original signals [43]. We extracted the features of EMG signals using root mean square (RMS) values and the coefficients of 6th-order autoregressive (AR) models [44,45].

D. Decoder Development

1) Decoder Architecture

The architecture of the proposed decoder was formed with the sequence input layer, LSTM neural network, fully connected layer, dropout layer, again fully connected layer, and regression layer in turn. The sequence input layer transferred the sequence data (EMG features) to the LSTM network. A delay of 48 ms (due to the inherent delay of the EMG sensors we employed) was incorporated with the EMG signals to account for the electromechanical delay from muscle activation to the resulting force production. The two fully connected layers linked every output element in the previous step with every input element in the next step. The output size of the first fully connected layer was set as 150, while the output size of the second one was set as 2. The dropout layer set input elements to zero randomly, with a probability of 0.5. The regression layer dealt with the regression problem between the actual and predicted values of angle and torque. The architecture of the proposed decoding strategy is presented in Fig. 2.

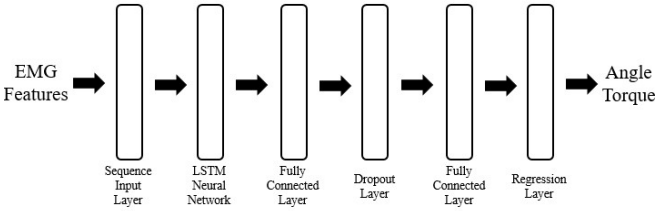

Fig. 2. The architecture of the proposed decoding strategy. The proposed decoder consists of multiple steps between the input (EMG features) and output (joint angle and torque); EMG features go through the sequence of input layer, LSTM neural network, fully connected layer, dropout layer, fully connected layer again, and regression layer. The angle and torque estimations are achieved through this procedure.

During the training phase, the decoder was trained with the EMG features as the input and the profiles of joint angle and torque as the output. These features (2 RMS values+12 coefficients of AR models) were extracted from EMG signals with a time window, while the profiles of joint angle and torque were averaged over the time window. We confirmed that the best performance was made when the number of the coefficients of AR models was 12 in a preliminary study. During evaluation, the trained decoder estimated the profiles of joint angle and torque according to the EMG features that were extracted from EMG signals with the time window.

In this study, the time window was set as 100 ms. In a preliminary study we found that the time window of 100 ms provided the best performance of the proposed method for prediction accuracy. The number of hidden units in the LSTM neural network was set to be 200. The number of the learnable parameters in the LSTM neural network was estimated as 136. No further notable improvement in estimation accuracy was seen beyond the number.

2) LSTM Neural Network

A unidirectional LSTM neural network consisted of an input layer, LSTM layer (hidden layer) and output layer

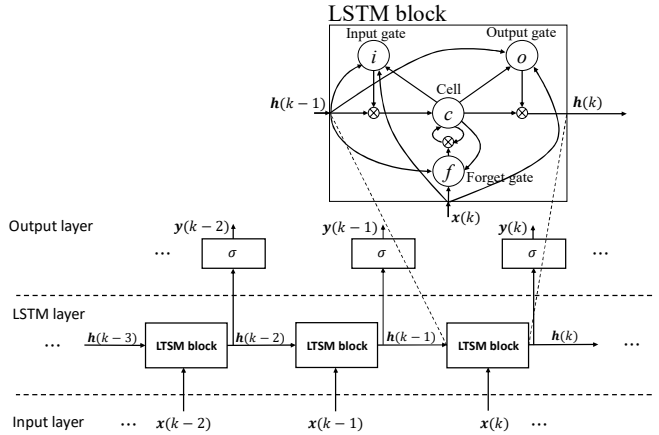

Fig. 3. A schematic of an (unidirectional) LSTM network. A relationship between the input vector $\boldsymbol{x}$ and output layer $\boldsymbol{y}$ is formed by activation vectors produced by the cell, and the input, output and forget gates. The input gate (i) modulates the input to the cell (c), the forget gate (f) allows the LSTM block to forget the previous memory, and the output gate (o) determines the output of the hidden layer.

(see Fig. 3). The LSTM layer was filled with multiple LSTM blocks that included a cell with self-connections for storing temporal states and a pair of adaptive, multiplicative gating units. The cell (c) was responsible for tracking the dependencies between the elements in the input sequence. The forget gate (f) was responsible for removing information from the cell state once the information was out of date. The input and output activations were controlled by the input gate (i) and output gate (o). The input gate governed a new value that flows into the cell, while the output gate governed the value in the cell that was used to compute the output activation.

While unidirectional LSTM neural networks learn the time dependencies of the input data that are chronologically ordered in a positive direction from time step $k-1$ to time step k, bidirectional LSTM neural networks additionally learn the dependencies of the reverse-chronological ordered input data to exploit more information. Fig. 4 depicts a bidirectional LSTM network that consists of a backward layer as well as a forward layer

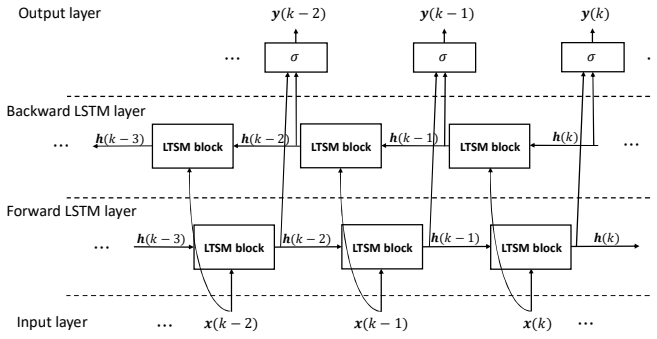

Fig. 4. A schematic of a bidirectional LSTM network. A bidirectional LSTM network consists of a backward layer and a forward layer to learn the backward and forward dependencies of the input data.

to learn the backward and forward dependencies of the input data.

Through the sequence input layer, EMG features (vector $\boldsymbol{x} \in \mathbf{R}^{\alpha}$) were admitted by the LSTM neural network and outputs (vector $\boldsymbol{y} \in \mathbf{R}^{\beta}$) were processed that led to the corresponding angle and torque through the fully connected layer, dropout layer, and regression layer. The dimensions α and β denoted the number of input features (14: 2 RMS values and 12 coefficients of AR models) and number of hidden units (200), respectively. A relationship between vector $\boldsymbol{x}$ and vector $\boldsymbol{y}$ at time point k of the LSTM neural network was identified using the following equations:

$$\boldsymbol{i}_k = \sigma(\boldsymbol{W}_i \boldsymbol{x}_k + \boldsymbol{U}_i \boldsymbol{h}_{k-1} + \boldsymbol{b}_i), \quad (1)$$
$$\boldsymbol{f}_k = \sigma(\boldsymbol{W}_f \boldsymbol{x}_k + \boldsymbol{U}_f \boldsymbol{h}_{k-1} + \boldsymbol{b}_f), \quad (2)$$
$$\boldsymbol{o}_k = \sigma(\boldsymbol{W}_o \boldsymbol{x}_k + \boldsymbol{U}_o \boldsymbol{h}_{k-1} + \boldsymbol{b}_o), \quad (3)$$
$$\boldsymbol{c}_k = \boldsymbol{f}_k \circledcirc \boldsymbol{c}_{k-1} + \boldsymbol{i}_k \circledcirc \tanh(\boldsymbol{W}_c \boldsymbol{x}_k + \boldsymbol{U}_c \boldsymbol{h}_{k-1} + \boldsymbol{b}_c), \quad (4)$$
$$\boldsymbol{h}_k = \boldsymbol{o}_k \circledcirc \tanh(\boldsymbol{c}_k), \quad (5)$$
$$\boldsymbol{y}_k = \boldsymbol{U}_y \boldsymbol{h}_k + \boldsymbol{b}_y, \quad (6)$$

where $\sigma(\cdot)$ is the sigmoid function and the operator $\circledcirc$ is the scalar product of two vectors. $\boldsymbol{i}$, $\boldsymbol{f}$, $\boldsymbol{o}$, and $\boldsymbol{c} \in \mathbf{R}^{\beta}$ denote the activation vectors of the input, forget, output, and cell gates, respectively. $\boldsymbol{h} \in \mathbf{R}^{\beta}$ denotes the hidden state of the hidden layer. The input weight matrices $\boldsymbol{W} \in \mathbf{R}^{\beta \times \alpha}$ quantifies the connection of the input vector $\boldsymbol{x}$ with the input state $\boldsymbol{i}$, forget state $\boldsymbol{f}$, output state $\boldsymbol{o}$, cell state $\boldsymbol{c}$, or output $\boldsymbol{y}$. The recurrent weight matrices $\boldsymbol{U} \in \mathbf{R}^{\beta \times \beta}$ quantifies the connection of the hidden state $\boldsymbol{h}$ with the input gate $\boldsymbol{i}$, forget gate $\boldsymbol{f}$, output gate $\boldsymbol{o}$, cell state $\boldsymbol{c}$, or output vector $\boldsymbol{y}$. The vector $\boldsymbol{b} \in \mathbf{R}^{\beta}$ denotes the biases of these connections.

For neural network training, a total of 180 epochs within which a satisfactory performance could be achieved were used. The loss function between the measured values $\boldsymbol{y}$ and the predictions $\hat{\boldsymbol{y}}$ was employed as

$$L = \frac{1}{N}\sum_{n=1}^{N}\left(\frac{1}{R}\sum_{i=1}^{R}|\boldsymbol{y_{ni}} - \hat{\boldsymbol{y}}_{\boldsymbol{ni}}|\right), \quad (7)$$

where N is the number of observations and R is the number of responses.

E. Experiment procedure

The experiment was composed of 3 stages in each of which different magnitudes of resistance were imposed on the wrist joint by the wrist robot. In the first stage, the robot was designed to produce minimized resistance (Soft), using an impedance control technique derived from the one (rigid mode) presented in [32], while resistance with a stiffness of 0.005 Nm/deg (Less Hard) and 0.03 Nm/deg (Hard) was imposed for the second and third stages, respectively, using proportional control (P control, see Fig. 5). The resistive torque was 0 at the neutral position of the wrist joint. To overcome the resistance by the robot, the participants need to generate a sufficient magnitude of torque at the joint through contraction of the agonist muscles. As well, they are required to modulate joint stiffness to follow the given trajectory as accurately as possible through co-contraction

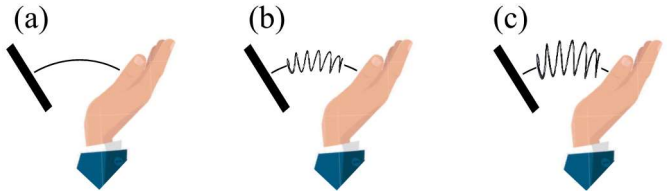

Fig. 5. Schematics of wrist joint movements in the presence of (a) zero resistance, (b) resistance with a stiffness of 0.005 Nm/deg and (c) resistance of 0.02 Nm/deg. The resistive torque is 0 at the neutral position (black thick line) of the wrist joint.

of the agonist-antagonist muscles. By imposing different magnitudes of resistance, we assess the performance of the proposed technique to decode joint torque as well as joint angle, and accordingly, joint stiffness. Each stage consisted of a training phase and evaluation phase, and each phase lasted about 80 seconds. A break time of 2 minutes was provided after each phase to mitigate the fatigue effect.

All participants sat on a chair in a comfortable posture but with a specific arm configuration on the right side: 45 degree abduction and 45 degree flexion in the shoulder, 50 degree flexion in the elbow. We set the neutral position of the wrist joint as 0 degrees. Participants were asked to move their right wrist joint, tracking a respective given trajectory for each phase (Fig. 6). These trajectories were generated using the X signal of a chaotic system to be irregular, aperiodic and of wide bandwidth [33]. The chaotic system is equated as:

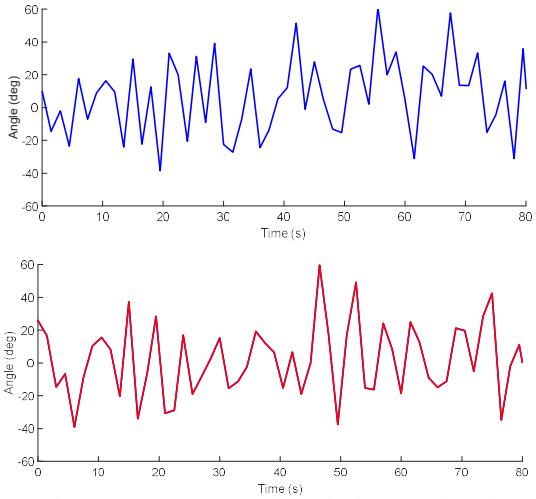

Fig. 6. Examples of trajectories given for each phase: (a) the training phase and (b) evaluation phase. Different trajectories are generated using a chaotic system by modulating its initial values. An angle of 0 degrees indicates the neutral position of the wrist joint. An angle of positive values is during extension, whereas an angle of negative values is during flexion.

$$\begin{aligned} \dot{x} &= \mathrm{a}(\mathrm{y}-\mathrm{x}), \\ \dot{y} &= -\mathrm{xz}+\mathrm{cy}, \\ \dot{z} &= y^2 - bz, \end{aligned} \tag{8}$$

where the parameters were selected as a = 35, b = 3, and c = 25 (employed from [33]).

The amplitude of the trajectories was bounded at ±50 degrees and their back-and-forth movement frequency was within about 0.6 Hz. The range of the amplitude covers the range of motion of the wrist joint for activities of daily living [34], the designed motion speed, which varied with time, can be regarded modest in daily life, based on [35].

F. Performance Evaluation

First, we analyzed the outcomes of the experiment. Means by each case across trial of the RMS values of the angle and torque calculated over each time window were evaluated to compare wrist joint displacements and torque generation according to the extent of resistance. To estimate changes in wrist joint stiffness according to the increases in resistance by the robot, the averaged instantaneous stiffness (partial derivative of the torque versus angle curve) was calculated.

To assess similarity in each participant between the data acquired during training and the data acquired during evaluation, we utilized the 12 coefficients of the AR model of EMG signals. Different inputs meant different outputs (i.e. angle and torque). By comparing the values of the coefficients of EMG signals for each time window during training with those of the corresponding coefficients for every time window during evaluation, we examined whether or not the data used to train the decoder were used for the evaluation phase. Similarity can be indexed as the minimum value of the summations of the differences in the values of the 12 coefficients throughout all time windows between the training and evaluation phases. While the difference in the values for each coefficient was ranged within 0 and 1, the index of 0 indicated that at least one same input of EMG existed in both the training and evaluation phases.

To evaluate the performance of the proposed decoding method with the unidirectional LSTM and bidirectional LSTM, a single decoder for each individual was trained with EMG features as the input and with joint angle and torque data as the output acquired throughout the training phase. The performance of the decoding strategy was evaluated by examining how accurately the joint angle and torque were predicted, respectively, by the trained decoder based on EMG signals during the evaluation phase. The variance accounted for (VAF) between the measured and predicted joint angle and between the measured joint torque and predicted joint torque was computed, respectively. The VAF is defined as

$$\mathrm{VAF} = \left(1 - \frac{variance(y-\hat{y})}{variance(y)}\right), \tag{9}$$

where y denotes measured values, while $\hat{y}$ denotes estimated values.

For a comparative study, RNN and a generalized linear model (GLM) [24] for the regression problem were selected. While the same feature extraction (explained above) was used, the raw EMG signals were bandpass filtered (20-400 Hz) for a better performance of GLM. The time window was set as 10 ms or 20 ms, across

subjects, for the RNN approach, while it was selected as 300 ms for the GLM approach, which produced the best performance. The number of hidden units in the RNN decoder was selected as 50. No further improvement in estimation accuracy was observed with more hidden units for RNN.

For the ease of data analysis, we first finished collecting all data and simulated the real-time circumstance to evaluate the online performance of the decoding technique. For evaluation, the acquired EMG data during the evaluation phase were read and processed to the EMG features in the LabVIEW program. The EMG features were then transferred via UDP to the decoder that had been trained in the secondary PC with the data acquired during the training phase, and the decoder sent out the predicted values back to the LabVIEW program. A comparison between the actual and predicted values (angle and torque) was made then.

G. Statistical Analysis

A repeated-measures analysis of variance (ANOVA), with case (three levels: Soft, Less Hard and Hard) as a within-subjects variable, was used to evaluate the degrees of movement, contact force and stiffness across repeated measurements. A mixed-design ANOVA, with case as a within-subjects variable and decoding method as a between-subjects variable, was employed to compare the performances of decoding approaches. If the sphericity assumption in ANOVAs was violated, then Greenhouse-Geisser adjusted p-values were used. Bonferroni post-hoc tests were conducted if pairwise comparisons were needed. The statistical analyses were performed with SPSS version 20.0 (SPSS Inc., Chicago, USA) and the significance level was set at 0.05. All analyses were preceded by Shapiro–Wilk tests of normality and their results were employed only when normality was not violated.

III. Results

First, we evaluated our experimental design that was aimed at eliciting different magnitudes of contact force and joint stiffness across cases while maintaining similar magnitudes of the angular displacement of the wrist joint (see Fig. 7).

It was reported that the mean across trial of the RMS values of the angle calculated over each time window had no significant main effect of case, implying that participants made similar amounts of movement during trials in each case.

ANOVA on the mean across trial of the RMS values of the torque calculated over each time window reported a significant main effect of case [$F(2,14)=1272.344$, $p < 0.001$]. Pairwise comparisons revealed significant differences between case Soft and case Less Hard ($p < 0.001$) and between case Less Hard and case Hard ($p < 0.05$). These results suggested that participants generated greater joint torque in case Hard to overcome the resistance by the robot than in case Less Hard that caused greater torque in comparison to case Soft.

ANOVA on stiffness revealed a significant main effect of case [$F(2,14)=97.040$, $p < 0.001$]. Pairwise comparisons revealed significant differences between case Soft and case Less Hard ($p < 0.001$) and between case Less Hard and case Hard ($p < 0.001$). These results suggested that participants employed stiffer wrist joint as the resistance by the robot was greater.

The similarity index for each participant was identified as a value above 0.276. These results indicated that none of the inputs used to train the decoder of each participant was the same as those used for evaluation.

With the new inputs that were not observed in the data sets for decoder training, the proposed decoding method in general showed an agreement of greater than 0.83 in VAF for angle estimation and an agreement of greater

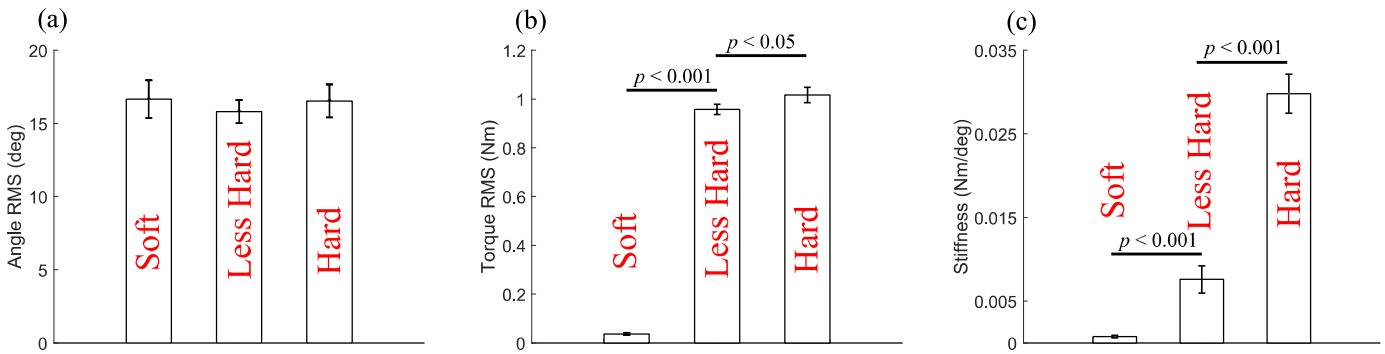

Fig. 7. Means by each case across trial of the RMS values of (a) the angle and (b) torque calculated over each time window, and (c) means by each case of instantaneous stiffness during the trial.

than 0.93 for torque estimation, between the actual and estimated variables, during interactions with an environment (cases Less Hard and Hard).

The proposed decoding technique incorporated with a unidirectional LSTM network produced a VAF of 0.8307±0.0176 (mean±s.d.) and 0.9105±0.0564 in average during cases Less Hard and Hard, respectively, while it produced a VAF of 0.8083±0.0107 in average during case Soft, for angle estimation. For torque estimation, a VAF of 0.9297±0.0034 and 0.9552±0.0010 in average was seen during cases Less Hard and Hard, respectively. VAFs between the measured and predicted joint torque for case Soft were not computed, since the noise component was dominant in measured joint torque for this case where the measured torque was assumed to be around zero. The noise component is difficult to be predicted by the proposed decoding method. Fig. 8 shows the results of a representative participant with the unidirectional LSTM. The trajectories of the original angle and torque and the corresponding trajectories averaged over the time window of 100 ms closely overlapped with each other. This implies that beside the 50ms electromechanical delay, there is no extra delay in

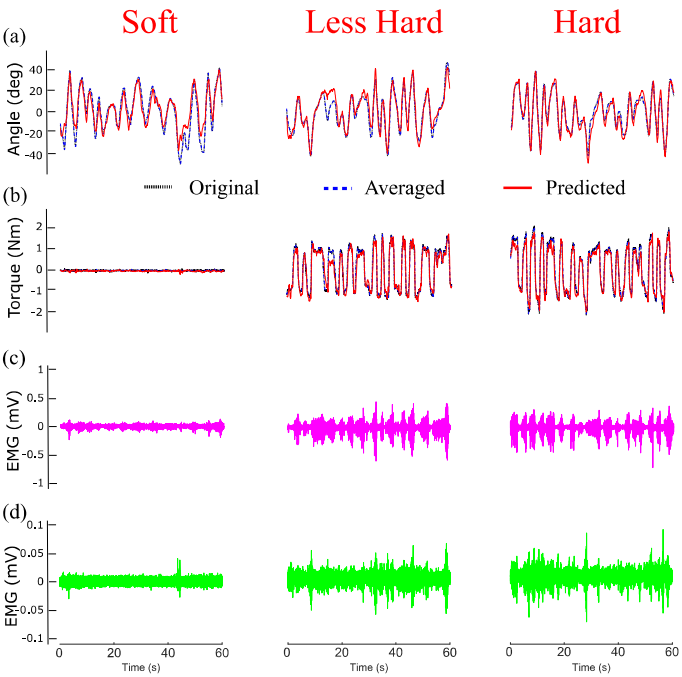

Fig. 8. Results by the unidirectional LSTM network of Subject 3. The trajectories of the measured and predicted joint angle (a) and the trajectories of the measured and predicted joint torque (b) for each case are displayed. The corresponding raw EMG signals of the ECR muscle (c) and FCR muscle (d) are presented. The proposed decoding method predicts the trajectory of the angle/torque averaged over the time window of 100 ms based on EMG signals, and the predicted trajectory (solid line) closely follows the trajectory (dashed line) of the original angle/torque (dotted line) averaged over the time window of 100 ms. The original trajectory and averaged trajectory closely overlap. The technique shows a VAF of 0.8845 and 0.9427 in the cases of Less Hard and Hard, respectively, while it shows a VAF of 0.8351 in the Soft case, for position estimation. For torque estimation, a VAF of 0.9459 and 0.9614 are recorded in the cases of Less Hard and Hard, respectively.

estimating outputs using the EMG features that were computed based on the past 150 to 50 ms EMG signals within the time window of 100 ms.

For the performance created by the bidirectional LSTM, a VAF of 0.8414±0.0331 and 0.8700±0.0373 in average for angle estimation was recorded during cases Less Hard and Hard, respectively. For torque estimation, a VAF of 0.9335±0.0193 and 0.9515±0.0168 in average was seen during cases Less Hard and Hard, respectively. The decoder with the bidirectional LSTM produced a VAF of 0.7231 in average for position estimation during case Soft. Fig. 9 displays the results of the representative participant with the bidirectional LSTM.

For RNN, a VAF of 0.5914±0.0923, 0.6200±0.0359 and 0.6508±0.0986 for angle estimation was seen during cases Soft, Less Hard and Hard, respectively. For torque estimation, a VAF of 0.8762±0.0100 and 0.8763±0.0129 was observed during cases Less Hard and Hard, respectively.

For GLM, a VAF of 0.2451±0.1210, 0.3435±0.0580 and 0.4924±0.0372 for angle estimation was recorded during cases Soft, Less Hard and Hard, respectively. For torque estimation, a VAF of 0.6755±0.0381 and 0.7324±0.0076 was seen during cases Less Hard and Hard, respectively.

ANOVA reported a significant main effect of decoding method for angle estimation [F(3,28) = 60.140, $p < 0.001$, η_P^2 =0.866]. Pairwise comparisons showed that there were no significant differences in performance between the unidirectional LSTM and bidirectional LSTM as the learning device of the proposed decoding methods, whereas these methods outperformed the methods with RNN and GLM ($p < 0.001$). A significant main effect of decoding method was observed for torque estimation [F(3,28) = 12.067, $p < 0.001$, η_P^2 =0.564]. Pairwise comparisons showed that there were no significant differences in performance among the unidirectional LSTM, bidirectional LSTM and RNN as a learning device while the method with GLM marked the lowest accuracy ($p < 0.005$). Significant differences between decoding methods for each case are displayed in Fig. 10.

ANOVA revealed a significant main effect of case for angle estimation [F(1.492,41.773) = 14.481, $p < 0.001$, η_P^2 =0.341] and torque estimation [F(1,28) = 7.550, $p < 0.05$, η_P^2 =0.212]. These results suggest that greater accuracy appears in case Hard than in case Less Hard and greater accuracy appears in case Less Hard than in case Soft for angle estimation while greater accuracy is exhibited in case Hard than in case Less Hard for torque estimation.

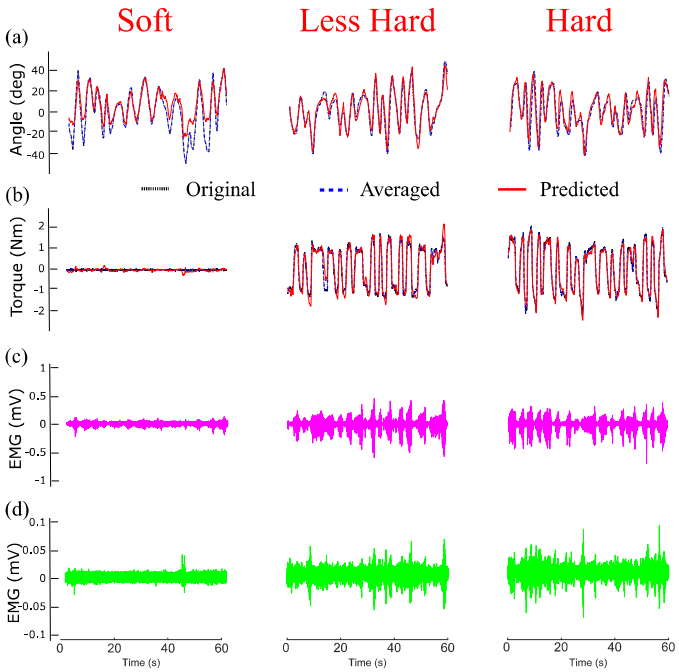

Fig. 9. Results by the bidirectional LSTM network of Subject 3. The trajectories of the measured and predicted joint angle (a) and the trajectories of the measured and predicted joint torque (b), and the corresponding raw EMG signals of the ECR muscle (c) and FCR muscle (d) are exhibited. The technique shows a VAF of 0.9284 and 0.9152 in the cases of Less Hard and Hard, respectively, while it shows a VAF of 0.7416 in the Soft case, for position estimation. For torque estimation, a VAF of 0.9305 and 0.9683 are recorded in the cases of Less Hard and Hard, respectively.

IV. Discussions

When we pick up either a tomato or an apple, different magnitudes of contact force are required, relying primarily on somatosensory feedback. If contact force is excessive, the fruit can burst. If contact force is insufficient, it can be dropped from the hand. All the while, movements of the fingers are involved in holding the object. Though it is possible for a robot manipulator or a computer-controlled prosthesis to deal with this problem through position/force hybrid control or impedance control, both 'contact force' and 'position' must be in control of the user when the operation is driven by the user's biological signals.

In this study, an EMG-based decoding method was proposed that predicts the position and torque of the wrist joint simultaneously. Numerous attempts have been made in an effort to decipher the user's intention through EMG interfaces [3, 10, 16, 36, 37], but the majority of these techniques tends to be concentrated on human movement decoding, despite the need of consideration in design of interactions with environments. Relatively few studies have been launched to develop decoding strategies that predict both kinematics and kinetics (or stiffness).

In our experiments, three levels of resistance were imposed on the wrist joint, while participants tracked the given trajectories with similar amplitudes. As resistance increased, it was required for participants to generate greater torque to overcome resistance through contraction of the agonist muscles. Meanwhile, it was required to modulate joint stiffness to follow the given trajectory as accurately as possible through contraction of the antagonist muscles, balancing it with contraction of the agonist muscles [38-40]. Therefore, the experiment design is thought to provide an insight into human motor control in terms of joint movement as well as joint stiffness during a given task. Indeed, the results showed that torque production increased as greater resistance was imposed on the wrist, while the amplitudes of joint movement remained the similar across cases. Correspondingly, joint stiffness increased to counteract the increased resistance by the robot.

Overall, the proposed decoding method produces an agreement of greater than 93% in torque estimation and an agreement of greater than 83% in angle estimation, between the actual and estimated values, during interactions with an environment. The proposed decoder based on (unidirectional or bidirectional) LSTM neural networks is superior in estimation performance to the decoders based on RNN and GLM, as presented in Fig. 9. In particular, the decoders with LSTM neural networks

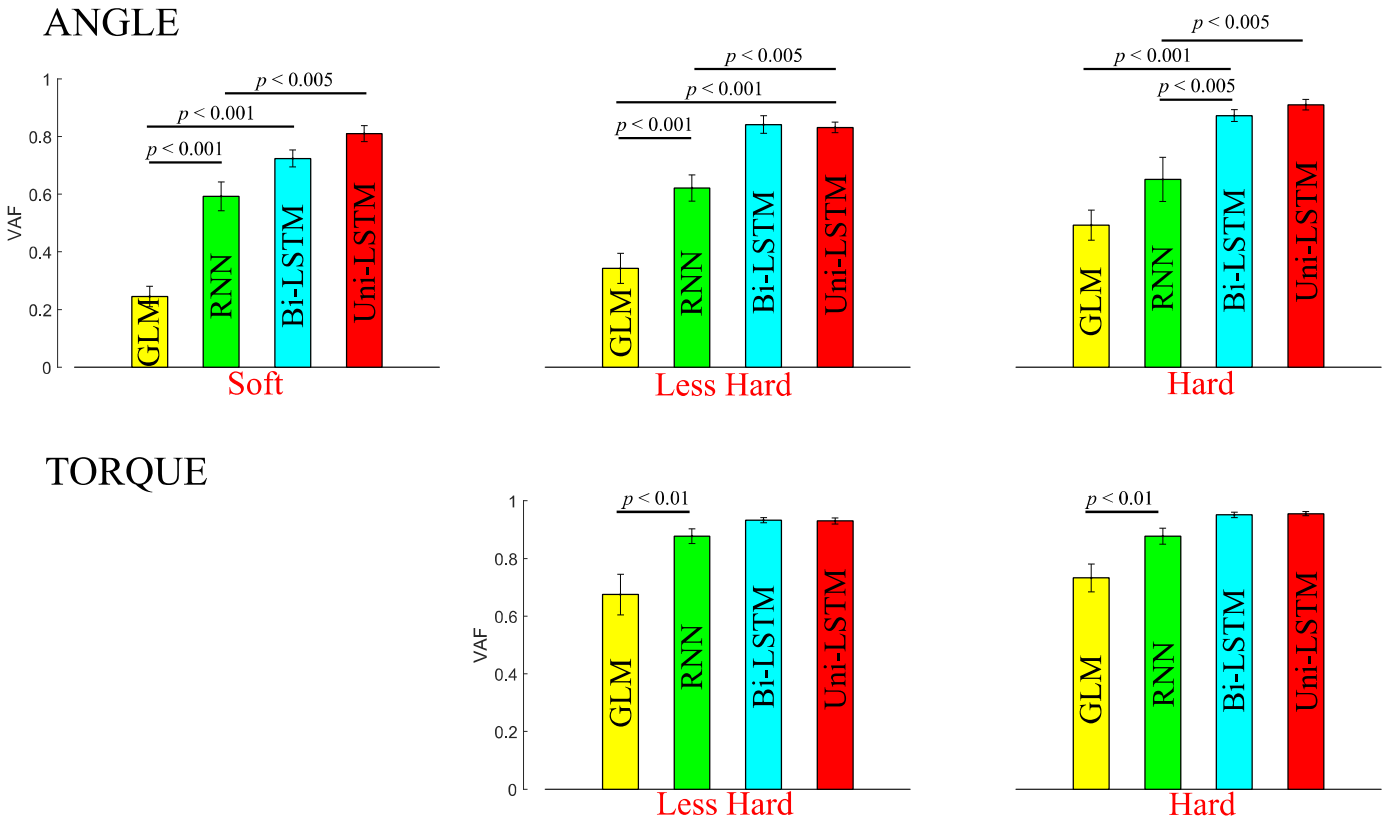

Fig. 10. A comparison of the proposed decoders incorporated with the unidirectional LSTM and bidirectional LSTM with the decoders based on RNN and GLM. VAFs averaged across all participants for each case and the corresponding standard deviations are presented. VAFs between the measured and predicted joint torque for case Soft are not evaluated; the noise component that is difficult to be predicted is dominant in measured joint torque for CASE 1 where the measured torque is nearly zero in the ideal condition.

produce significantly greater accuracy in angle estimation, in comparison with the decoders based on RNN and GLM ($p < 0.05$).

Accuracy is greater in estimations of the angle and torque during case Hard, followed by cases Soft and Less Hard in turn ($p < 0.05$). It may be because stronger resistance causes more muscle activation while achieving movements of the same amplitude, which makes clear the difference between the phases of contraction and non-contraction of the target muscle.

The proposed decoding method employed a machine learning technique. Machine learning has recently attracted extraordinary attention as a tool highly efficient to relate two parties that look difficult to be related. Several studies demonstrated the superiority of neural networks in myoelectrically driven applications using surface EMG [10, 16-20]. In particular, LSTM neural networks are able to automatically determine the optimal time lags and learn the time series with longtime spans. Indeed, our proposed method estimated participants' movement and force with an excellent agreement, though the decoder was not trained with the similar trajectories used for evaluation. As observed in Fig. 6, the two trajectories for the training and evaluation phases, respectively, are highly irregular, aperiodic and different from each other. The two trajectories lead to inputs for the training phase that are not shared with those for the evaluation phase. These results imply the strength of the proposed method that is based on what the decoder is trained using varying time lags in estimating the angle and torque with new inputs resulting from a series of different trajectories of motion [41]. In our related study, we demonstrated that the decoding strategy with LSTM neural networks is superior in coping with the data with a long-time span [31]. This feature is advantageous in that unlearned trajectories of motion can be predicted from learned trajectories of motion.

The suitability and superiority of the proposed method that employs LSTM neural networks in EMG-based decoding tasks are pronounced from the comparisons with the decoders that employ RNN and GLM. RNN is characterized by fixed time lags in training. Lower accuracy of the RNN decoder implies that varying time lags in training is more efficient in learning biological signals than fixed time lags. The results of the decoder with GLM indicates the lack of the capability in the regression-based method to deal with the time dependency of EMG signals. This method searches the coefficients of the regression model through the

relationships of the input and output at the same time point.

We showed no significant differences in performance between the decoder with the unidirectional LSTM and the decoder with the bidirectional LSTM. Unidirectional LSTM neural networks make use of only the forward dependency of time series data which are chronologically arranged. Meanwhile, bidirectional LSTM neural networks make use of both the forward and backward dependencies of data. It was reported that in the case that the time series data show periodicity and regularity, bidirectional LSTM neural networks outperform unidirectional LSTM neural networks [42]. The fact that our data are highly irregular and aperiodic primarily leads to no significant differences in performance between the two decoders.

V. Conclusion

We have proposed an EMG-based decoding technique for simultaneous estimation of the position and torque of a joint of the limb in interaction with environments, employing LSTM neural networks. The proposed method that admits the advantages of LSTM networks showed superior performance in simultaneous estimation of the position and torque by dealing with high time dependency of EMG inputs. The decoding results showed an agreement of greater than 93% in torque estimation and an agreement of greater than 83% in angle estimation, between the actual and estimated values, during interactions with an environment. Through a comparative study, we demonstrated the suitability and superiority of the proposed method based on LSTM neural networks with the capability of learning a long time-span data with varying time lags.

Sources of Funding

This research study was supported by the National Institute on Disability, Independent Living, and Rehabilitation Research (Grant # 90DP0099). The first author was also supported by the University of Maryland Baltimore Institute for Clinical and Translational Research (ICTR) which is funded in part by Grant Number TL1 TR003100 from the National Center for Advancing Translational Sciences (NCATS) a component of the National Institutes of Health (NIH), and NIH Roadmap for Medical Research.

Disclosures

L-Q Zhang has an ownership in Rehabtek LLC, which received U.S. federal funding in developing the rehabilitation robot used in this study. This study was completed in conflict between D Kim and L-Q Zhang regarding discrimination and retaliation matters.

References

[1] A. T. Au and R. F. Kirsch, "EMG-based prediction of shoulder and elbow kinematics in able-bodied and spinal cord injured individuals," *IEEE Trans Rehabil Eng,* vol. 8, no. 4, pp. 471-80, Dec 2000. [Online]. Available: https://www.ncbi.nlm.nih.gov/pubmed/11204038.

[2] D. Song *et al.*, "Predicting EMG with generalized Volterra kernel model," *Conf Proc IEEE Eng Med Biol Soc,* vol. 2008, pp. 201-4, 2008, doi: 10.1109/IEMBS.2008.4649125.

[3] C. L. Pulliam, J. M. Lambrecht, and R. F. Kirsch, "Electromyogram-based neural network control of transhumeral prostheses," *J Rehabil Res Dev,* vol. 48, no. 6, pp. 739-54, 2011. [Online]. Available: https://www.ncbi.nlm.nih.gov/pubmed/21938659.

[4] P. Liu, L. Liu, F. Martel, D. Rancourt, and E. A. Clancy, "Influence of joint angle on EMG-torque model during constant-posture, quasi-constant-torque contractions," *J Electromyogr Kinesiol,* vol. 23, no. 5, pp. 1020-8, Oct 2013, doi: 10.1016/j.jelekin.2013.06.011.

[5] X. Li, H. Shin, P. Zhou, X. Niu, J. Liu, and W. Z. Rymer, "Power spectral analysis of surface electromyography (EMG) at matched contraction levels of the first dorsal interosseous muscle in stroke survivors," *Clin Neurophysiol,* vol. 125, no. 5, pp. 988-94, May 2014, doi: 10.1016/j.clinph.2013.09.044.

[6] D. Staudenmann, I. Kingma, D. F. Stegeman, and J. H. van Dieen, "Towards optimal multi-channel EMG electrode configurations in muscle force estimation: a high density EMG study," *J Electromyogr Kinesiol,* vol. 15, no. 1, pp. 1-11, Feb 2005, doi: 10.1016/j.jelekin.2004.06.008.

[7] A. M. Simon, K. Stern, and L. J. Hargrove, "A comparison of proportional control methods for pattern recognition control," *Conf Proc IEEE Eng Med Biol Soc,* vol. 2011, pp. 3354-7, 2011, doi: 10.1109/IEMBS.2011.6090909.

[8] B. Peerdeman *et al.*, "Myoelectric forearm prostheses: state of the art from a user-centered perspective," *J Rehabil Res Dev,* vol. 48, no. 6, pp. 719-37, 2011. [Online]. Available: https://www.ncbi.nlm.nih.gov/pubmed/21938658.

[9] J. M. Hahne *et al.*, "Linear and nonlinear regression techniques for simultaneous and proportional myoelectric control," *IEEE Trans Neural Syst Rehabil Eng,* vol. 22, no. 2, pp. 269-79, Mar 2014, doi: 10.1109/TNSRE.2014.2305520.

[10] J. Liu, S. H. Kang, D. Xu, Y. Ren, S. J. Lee, and L. Q. Zhang, "EMG-Based Continuous and Simultaneous Estimation of Arm Kinematics in Able-Bodied Individuals and Stroke Survivors," *Front Neurosci,* vol. 11, p. 480, 2017, doi: 10.3389/fnins.2017.00480.

[11] W. Sun, J. Zhu, Y. Jiang, H. Yokoi, and Q. Huang, "One-Channel Surface Electromyography Decomposition for Muscle Force Estimation," *Front Neurorobot,* vol. 12, p. 20, 2018, doi: 10.3389/fnbot.2018.00020.

[12] S. Rao, R. Carloni, and S. Stramigioli, "Stiffness and position control of a prosthetic wrist by means of an EMG interface," *Conf Proc IEEE Eng Med Biol Soc,* vol. 2010, pp. 495-8, 2010, doi: 10.1109/IEMBS.2010.5627153.

[13] E. Hocaoglu and V. Patoglu, "Tele-impedance control of a variable stiffness prosthetic hand," in *2012 IEEE International Conference on Robotics and Biomimetics (ROBIO)*, 2012: IEEE, pp. 1576-1582.

[14] C. W. Antuvan and L. Masia, "Position and stiffness modulation of a wrist haptic device using myoelectric interface," *IEEE Int Conf Rehabil Robot,* vol. 2017, pp. 734-739, Jul 2017, doi: 10.1109/ICORR.2017.8009335.

[15] P. K. Artemiadis and K. J. Kyriakopoulos, "EMG-based position and force estimates in coupled human-robot systems: Towards EMG-controlled exoskeletons," in *Experimental Robotics*, 2009: Springer, pp. 241-250.

[16] S. Muceli and D. Farina, "Simultaneous and proportional estimation of hand kinematics from EMG during mirrored movements at multiple degrees-of-freedom," *IEEE Trans Neural Syst Rehabil Eng,* vol. 20, no. 3, pp. 371-8, May 2012, doi: 10.1109/TNSRE.2011.2178039.

[17] N. Jiang, S. Muceli, B. Graimann, and D. Farina, "Effect of arm position on the prediction of kinematics from EMG in amputees," *Medical & biological engineering & computing,* vol. 51, no. 1-2, pp. 143-151, 2013.

[18] M. Atzori, M. Cognolato, and H. Müller, "Deep learning with convolutional neural networks applied to electromyography data: A resource for the classification of movements for prosthetic hands," *Frontiers in neurorobotics,* vol. 10, p. 9, 2016.

[19] P. Xia, J. Hu, and Y. Peng, "EMG-based estimation of limb movement using deep learning with recurrent convolutional neural networks," *Artificial organs,* vol. 42, no. 5, pp. E67-E77, 2018.

[20] M. Zia ur Rehman *et al.*, "Multiday EMG-based classification of hand motions with deep learning techniques," *Sensors,* vol. 18, no. 8, p. 2497, 2018.

[21] Y. Fang, D. Zhou, K. Li, Z. Ju, and H. Liu, "Attribute-Driven Granular Model for EMG-Based Pinch and Fingertip Force Grand Recognition," *IEEE Trans Cybern,* Aug 16 2019, doi: 10.1109/TCYB.2019.2931142.

[22] L. H. Smith, L. J. Hargrove, B. A. Lock, and T. A. Kuiken, "Determining the optimal window length for pattern recognition-based myoelectric control: balancing the competing effects of classification error and controller delay," *IEEE Trans Neural Syst Rehabil Eng,* vol. 19, no. 2, pp. 186-92, Apr 2011, doi: 10.1109/TNSRE.2010.2100828.

[23] R. Menon, G. Di Caterina, H. Lakany, L. Petropoulakis, B. A. Conway, and J. J. Soraghan, "Study on interaction between temporal and spatial information in classification of EMG signals for myoelectric prostheses," *IEEE Transactions on Neural Systems and Rehabilitation Engineering,* vol. 25, no. 10, pp. 1832-1842, 2017.

[24] J. Liu, Y. Ren, D. Xu, S. H. Kang, and L.-Q. Zhang, "EMG-Based Real-Time Linear-Nonlinear Cascade Regression Decoding of Shoulder, Elbow and Wrist Movements in Able-Bodied Persons and Stroke Survivors," *IEEE Trans Biomed Eng,* vol. 67, no. 5, pp. 1272-1281, 2020.

[25] F. A. Gers, J. Schmidhuber, and F. Cummins, "Learning to forget: Continual prediction with LSTM," 1999.

[26] S. Hochreiter and J. Schmidhuber, "Long short-term memory," *Neural Comput,* vol. 9, no. 8, pp. 1735-80, Nov 15 1997. [Online]. Available: https://www.ncbi.nlm.nih.gov/pubmed/9377276.

[27] A. Graves, A.-r. Mohamed, and G. Hinton, "Speech recognition with deep recurrent neural networks," in *2013 IEEE international conference on acoustics, speech and signal processing*, 2013: IEEE, pp. 6645-6649.

[28] A. Graves and J. Schmidhuber, "Framewise phoneme classification with bidirectional LSTM and other neural network architectures," *Neural Netw,* vol. 18, no. 5-6, pp. 602-10, Jun-Jul 2005, doi: 10.1016/j.neunet.2005.06.042.

[29] M. Baccouche, F. Mamalet, C. Wolf, C. Garcia, and A. Baskurt, "Sequential deep learning for human action recognition," in *International workshop on human behavior understanding*, 2011: Springer, pp. 29-39.

[30] J. Kumar, R. Goomer, and A. K. Singh, "Long short term memory recurrent neural network (lstm-rnn) based workload forecasting model for cloud datacenters," *Procedia Computer Science,* vol. 125, pp. 676-682, 2018.

[31] D. Kim *et al.*, "Simultaneous Estimations of Joint Angle and Torque in Interactions with Environments using Electromyography," presented at the International Conference on Robotics and Automation (ICRA), Paris, May 31 - June 4, 2020.

[32] D. Kim, K. Koh, G.-R. Cho, and L.-Q. Zhang, "A Robust Impedance Controller Design for Series Elastic Actuators using the Singular Perturbation Theory," *IEEE/ASME Transactions on Mechatronics,* vol. 25, no. 1, pp. 164-174, 2020, doi: 10.1109/TMECH.2019.2951417.

[33] D. Kim, P. H. Chang, and S.-h. Kim, "A new chaotic attractor and its robust function projective synchronization," *Nonlinear Dynamics,* vol. 73, no. 3, pp. 1883-1893, 2013.

[34] A. K. Palmer, F. W. Werner, D. Murphy, and R. Glisson, "Functional wrist motion: a biomechanical study," *Journal of Hand Surgery,* vol. 10, no. 1, pp. 39-46, 1985.

[35] K. A. Mann, F. W. Wernere, and A. K. Palmer, "Frequency spectrum analysis of wrist motion for activities of daily living," *Journal of Orthopaedic research,* vol. 7, no. 2, pp. 304-306, 1989.

[36] R. Song, K.-y. Tong, X. Hu, and L. Li, "Assistive control system using continuous myoelectric signal in robot-aided arm training for patients after stroke," *IEEE transactions on neural systems and rehabilitation engineering,* vol. 16, no. 4, pp. 371-379, 2008.

[37] A. Smith and E. E. Brown, "Myoelectric control techniques for a rehabilitation robot," *Applied Bionics and Biomechanics,* vol. 8, no. 1, pp. 21-37, 2011.

[38] P. L. Gribble, L. I. Mullin, N. Cothros, and A. Mattar, "Role of cocontraction in arm movement accuracy," *Journal of neurophysiology,* vol. 89, no. 5, pp. 2396-2405, 2003.

[39] L. P. Selen, P. J. Beek, and J. H. Van Dieën, "Can co-activation reduce kinematic variability? A simulation study," *Biological cybernetics,* vol. 93, no. 5, pp. 373-381, 2005.

[40] L. P. Selen, P. J. Beek, and J. H. Van Dieën, "Impedance is modulated to meet accuracy demands during goal-directed arm movements," *Experimental Brain Research,* vol. 172, no. 1, pp. 129-138, 2006.

[41] S. Hochreiter and J. Schmidhuber, "Bridging long time lags by weight guessing and "Long Short-Term Memory"," *Spatiotemporal models in biological and artificial systems,* vol. 37, no. 65-72, p. 11, 1996.

[42] C. Cui *et al.*, "Simultaneous Recognition and Assessment of Post-Stroke Hemiparetic Gait by Fusing Kinematic, Kinetic, and Electrophysiological Data," *IEEE Transactions on Neural Systems and Rehabilitation Engineering,* vol. 26, no. 4, pp. 856-864, 2018, doi: 10.1109/TNSRE.2018.2811415.

[43] A. Phinyomark et al., "Feature extraction of the first difference of EMG time series for EMG pattern recognition," Comput. Methods Programs Biomed., vol. 117, pp. 247–256, Nov. 2014.

[44] R. Boostani and M. H. Moradi, "Evaluation of the forearm EMG signal features for the control of a prosthetic hand," Physiol. Meas., vol. 24, pp. 309–319, May 2003.

[45] D. Farina and R. Merletti, "Comparison of algorithms for estimation of EMG variables during voluntary isometric contractions," J. Electromyography Kinesiol., vol. 10, pp. 337–349, Oct. 2000